Electronic Supplementary Material (ESI) for Physical Chemistry Chemical Physics

Version: 20130121

SUPPORTING INFORMATION

Inkjet Printing as a Tool for the Patterned Deposition of Octadecylsiloxane Monolayers on Silicon Oxide Surfaces

Christian Belgardt, Enrico Sowade, Thomas Blaudeck, Thomas Baumgärtel,

Harald Graaf, Christian von Borczyskowski, Reinhard R. Baumann

Corresponding Author: Thomas Blaudeck, e-mail: thomas.blaudeck@physik.tu-chemnitz.de;

phone: +49.(0)371.531.35610

Chapter A.1: Growth principles of OTS-SAMs on silicon oxide surfaces

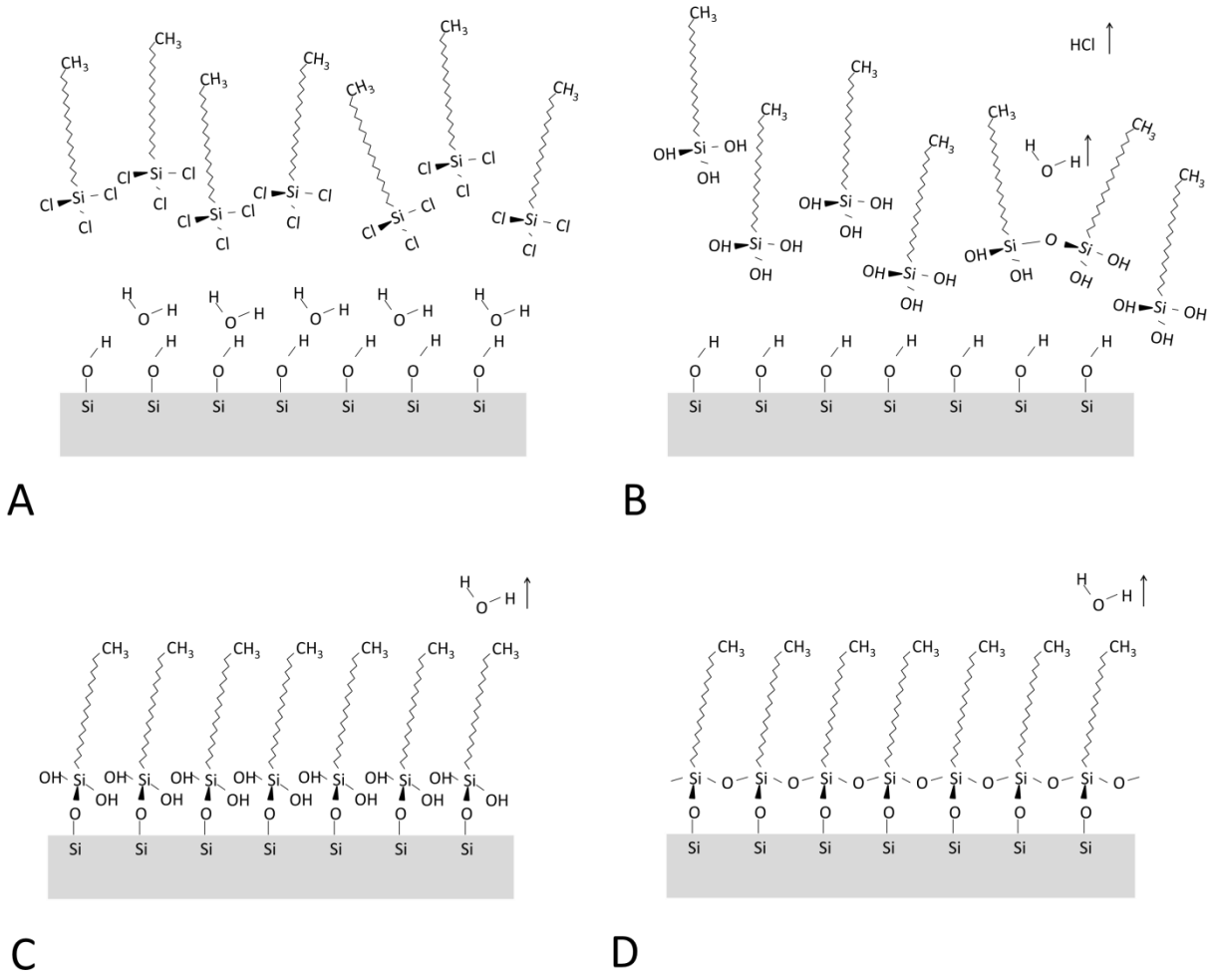

Figure A.1: Elementary physicochemical mechanisms of the formation of OTS-SAMs on silicon oxide surfaces according to Sagiv.[61] The cartoons of the molecules transferred to the gaseous phase are qualitative only, without considering the stoichiometry.

There are numerous experimental studies in literature on SAM formation and its kinetics, especially of island growth, with the help of atomic force microscopy (AFM), ellipsometry, infrared spectroscopy, or x-ray scattering. [10][11][12][13][14][15][54][55][56][57][58][59][60][61][62][63][64] Figure A.1 shows the mechanism for the formation of OTS-SAMs on silicon oxide surfaces based on Sagiv.[61] The whole growth process is initiated by a partial hydrolysis of silane molecules in the presence of water molecules.[61] The water molecules are either physisorbed on the hydroxylated silicon oxide surface (cf. Figure A.1A) or present in the solvent (see Figure A.1B). A minimum of three water

molecules per OTS molecule is necessary for a complete hydrolysis of the silane molecules. The water is released after the formation of the lateral bonds which initiates the formation of the monolayer (see Figure A.1C and D) and then present in the solvent. For nearly anhydrous liquids, the hydrolysis process in solution is slowed down so that there are only few hydroxylized silane molecules available for a later chemisorption which leads to an inhomogeneous monolayer formation[12] (see Figure A.2). For liquids with high water content, the hydroxylized silane molecules will polymerize completely in the carrier liquid bulk, forming clusters (as indicated in Fig. A1.B, left) or even closed-shell micelles that prevent the silane end groups from a later reaction with the silicon oxide surface and inhibit the formation of even disordered molecular monolayers. The process of hydroxylation is followed by a physisorption of the hydroxylized silane molecules (or partial clusters) on the hydroxylated silicon oxide surface. The molecules may undergo a planar diffusion on the silicon oxide surface until van der Waals forces between the hydrophobic alkyl chains of diffusing silane molecules and already sessile clusters (or larger islands) form domains of a self-assembled molecular monolayer (SAM)[10]. In principle, there are two different growth types for SAMs: (a) island formation and (b) formation from temporarily disordered molecular layers transferring to a more ordered monolayer. In case (a), diffusion of OTS molecules leads to small, smooth, single-layered, sharp-edged circular islands of OTS molecules standing upright on the substrate.[54][57] These islands have a diameter of approximately 100 nm and a height of 2.5 nm. The formation process is followed by a chemisorption of the molecules (see Figure A.1C) and the formation of lateral Si-O-Si bonds of undefined structure (see Figure A.1D) as confirmed by X-ray diffraction data[62] and reflectivity studies.[64] Especially the immobilization of the head group is decisive for the thermal stability of the SAM.[63] In the case (b), the formation of partial micelles in solution (see Figure A.1B) leads to the formation of considerably large planar aggregates on the substrate with a branched shape on account of a diffusion-limited growth mechanism. Here, the physisorbed, yet less mobile, planar aggregates grow by adsorption of other OTS molecules still diffusing on the silicon oxide surface.[58] This process resembles the well-known Ostwald ripening, as the planar aggregates from fragmental species.[15] In consequence, an extended immersion time results in planar aggregates larger in size but smaller in number per unit area. The layers grown in case b) are characterized by a residual disorder and inhomogeneity. Again, the formation process is finalized by a chemisorption of the molecules (see Figure A.1C), and the formation of lateral Si-O-Si bonds (see Figure A.1D),

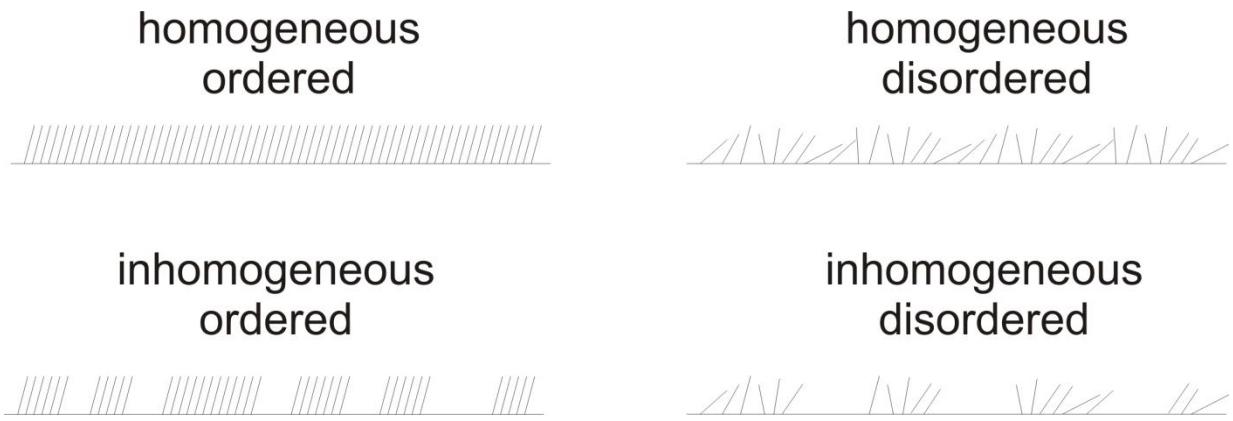

Figure A.2: Order types of monolayer structures

Chapter A.2: Growth of OTS-SAMs from solution for various solvents

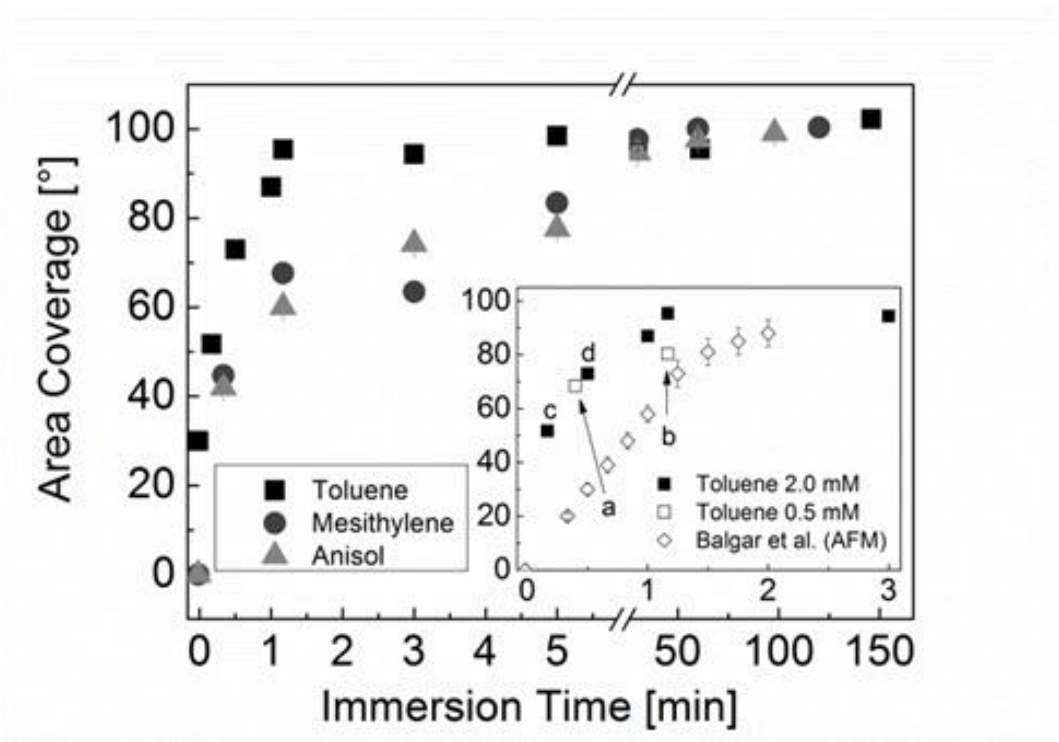

Figure A.3: SAM coverage on silicon oxide from chemical baths of toluene, mesitylene, and anisol (c = 0.5 mM; T = 25 °C, RH 53 %). Inset: comparison with results from Balgar et al. (cf. Ref. [15]).

In our experiments, the SAMs were grown from toluene at the same concentrations as the printing experiments were performed, i.e. at 0.5 mM and 2.0 mM. Conditions were kept at follows: temperature 25 °C, relative humidity (RH) 53 %. The substrates were taken from identical silicon wafers. They were immersed for different times and characterized with goniometry (water contact angle) and atomic-force microscopy (AFM). In the graph of Figure A.3, the effective area coverage (y-axis) was derived from Cassie's law from measurements of the water contact angle. The inset zooms into the results for short immersion times for toluene (c = 0.5 mM and c = 2.0 mM, T = 25 °C, RH 53 %) and compares with the results of Balgar et al. (cf. Ref. [15]) who used atomic-force microscopy (AFM) to determine the effective area coverage. The difference between immersion in toluene and mesitylene is as follows: in toluene the maximum water contact angle of 110° is reached after several minutes, it takes about an hour for mesitylene. This lower growth speed in mesitylene could tentatively be ascribed to the higher

viscosity of the mesitylene compared to toluene and hence a slower diffusion of the OTS molecules in the liquid.

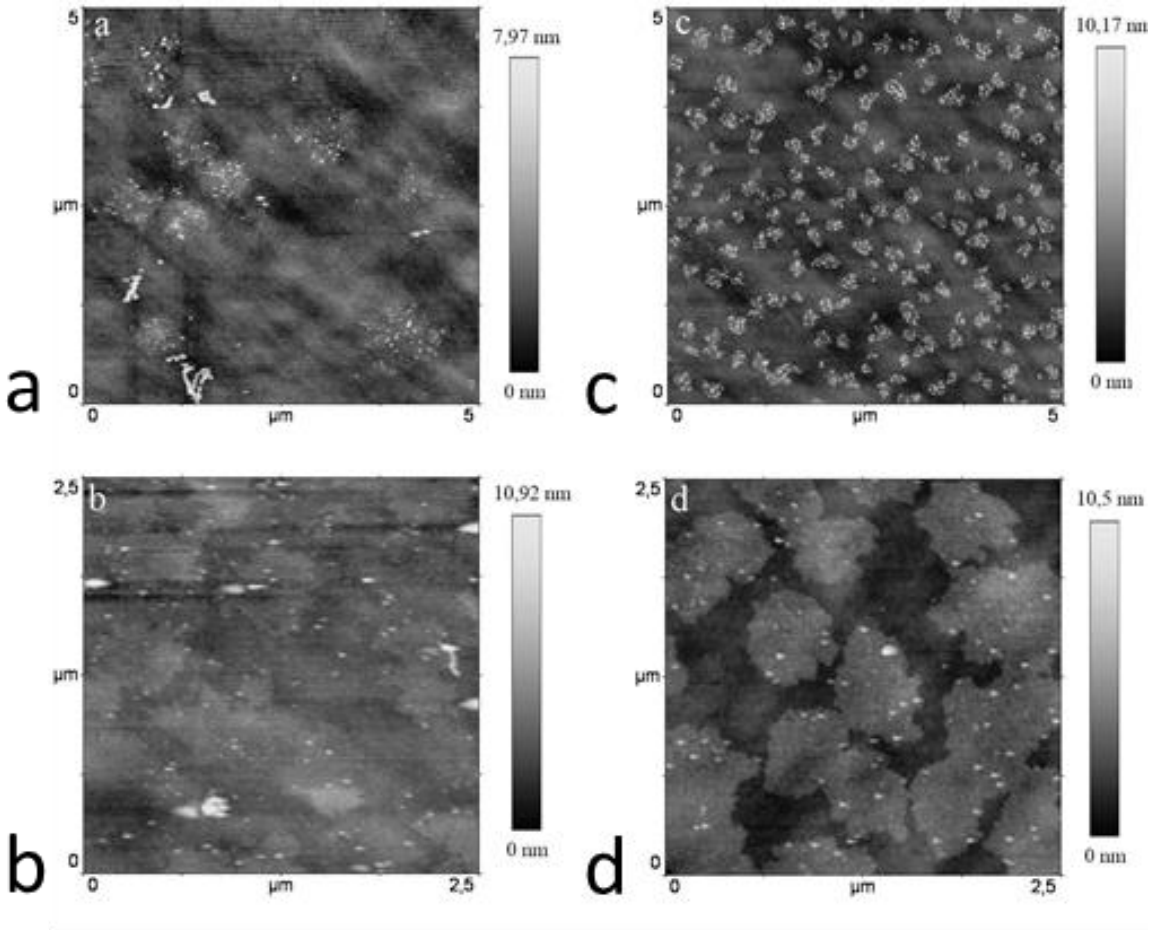

Figure A.4: AFM images of the OTS-SAM growth from a chemical bath of toluene

a) c = 0.5 mM; T = 25 °C; RH 53 %; t = 24 s;

b) c = 0.5 mM; T = 25 °C, RH 53 %; t = 70 s;

c) c = 2.0 mM; T = 25 °C; RH 53 %; t = 10 s;

d) c = 2.0 mM; T = 25 °C; RH 53 %; t = 30 s.

Figure A.4 shows AFM topography images of the OTS-SAM growth from a chemical bath of toluene for four data points of Figure A.3, i.e. at concentrations of 0.5 mM and 2.0 mM. The AFM topography exhibits the typical island growth: after 10 seconds immersion, islands with a

height of clearly less than 5 nm have formed (Fig. A.4c). At 30 seconds immersion time, the number density is reduced and the size is increased (Fig. A.4d). After 60 seconds immersion time, the silicon oxide surface appears flat in the AFM topography image. This means that the mean distance between the individual OTS molecules is lower than the diameter of the AFM tip apex (about 20 nm). As the samples exhibit a water contact angle of 100°, an area coverage of 80 % can be assumed. For the lower concentration of 0.5 mM, the island growth is less pronounced. The island density is lower than for the higher concentrated solution (Fig. A.4a). Even after 70 seconds, island growth cannot be observed (Fig. A.4b). The decisive role of the water for the SAM formation process has practical consequences for the storage of the ink fluid: a completely inert atmosphere such as nitrogen is inevitable as it prevents an accelerated aggregation of the molecules in solution. According to our experiences, at ambient conditions, a typical ink load of 2 mL will completely polymerize within one hour. Another way of storing is the usage of molecular sieves with a pore diameter of 4 Å (see Ref. [12]). Printing in a completely inert atmosphere is not recommended as the formation of molecular islands that are necessary to initiate the growth towards an ordered monolayer requires a certain number of water molecules. The ideal case would hence be an in-situ control of the water content of the carrier liquid (see Ref. [17]).

Chapter A.3: Properties of the OTS solvents and kinetics of the evaporation of small sessile droplets

Table A.1 contains several parameters of selected solvents for OTS. The vapor pressure was taken from data sheets of relevant suppliers (Merck KG, Sigma Aldrich). The jettability of the solvents is a subjective parameter deducted from the drop formation of the ejected droplets and was tested on several DMP-2831 (10 pL print heads) at both Chemnitz University of Technology and Printed Electronics Arena Manufacturing, Norrköping.

Table A.1: Vapor pressure and jettability of selected solvents and evaporation times for their sessile droplets: i) for a 50 nL sessile droplet measured by video microscopy and ii) estimated for a typical inkjet droplet of 10 pL

	Vapor pressure [hPa]	Jettability on DMP-2831	Evaporation time 50 nL [s]	Evaporation time 10 pL [ms]
Anisol	3.2	N/A	120	328
Mesitylene	2.8	good	136	451
Toluene	29	poor	14	44
o-Xylol	7.0	N/A	52	164
p-Xylol	8.7	N/A	43	147

In the right column of Table A.1, the evaporation times for 10 pL droplets were linearly extrapolated from the measured values for 50 nL. To this end, 50 nL droplets were placed on silicon oxide and its evaporation was observed by applying digital video equipment to a dataphysics OCA-20 goniometer and evaluating the video stream with a MATLAB script (see also Supporting Information, A.5). In order to estimate the role of line-tension effects for the evaporation kinetics we consulted the work of Fan[51] who describes the spreading evolution of small droplets. According to this author, the dynamics of the spreading of a micrometer-sized droplet is led by both the surface and line energies, whereas the volume contributions are negligible (i.e. gravity potential is not relevant). The total free energy can be written as

$$G = \Sigma \gamma_{ij} A_{ij} + \tau \cdot l - W = \gamma_{LV} A_{LV} + \gamma_{SV} A_{SV} + \gamma_{SL} A_{SL} + \tau \cdot l - W \qquad \text{(A.1)}$$

Here, γ_{ij} is the specific surface tension and A_{ij} is the area of the interface between phase i and phase j ($i, j \in \{S, L, V\}; i \neq j$). Consequently, τ is the line tension and l the length of the contact line representing the circumference of the base area. The external work supply is denoted by W. The author derives the radial velocity of the contact line v_L as

$$v_L \sim \gamma_{SV} - \gamma_{SL} - \gamma_{LV} \cos\theta - \frac{\tau}{R_l} \qquad \text{(A.2)}$$

with θ the contact angle and R_l the radius of the base area. We have to point out that this equation describes the spreading of a droplet which ends up in an outward movement indicated by a positive sign of v_L. For a transfer to our situation of a shrinking droplet due to evaporation-induced volume loss we assume that the droplet evaporates with constant or almost constant contact angle. It turns out that the radial velocity of the movement of the contact line is increasingly governed by the term bearing the line tension, as the radius of the base area decreases with progressing evaporation. This means that the process of evaporation is accelerated for sufficiently low radii of the base area thus that the linear extrapolation overestimated the immersion times for small droplets. However, it should not affect the discussion in the manuscript as this represents a reconfiguration of the abscissae in Figures 4 in the main paper which have to be compressed by a possibly non-linear, yet monotonous function.

Chapter A.4: Hydrophobicity of the printed areas

The hydrophobicities of the areas in which OTS ink droplets were deposited via inkjet are shown in two examples (Figures A.5 and A.6). In Figure A.5, the red rectangle indicates the position and the dimensions of (10x3) mm^2 of the printing area. Sprayed drops of deionized water indicate that in the printing area the contact angle is considerably larger than less than on the remaining parts of the surface. The blue line in Figure A.5B indicates the trajectory along which the water contact angles of Figure A.5A were measured. Figure A.6A and A.6B show a typical printing pattern with varying drop spacing and the photography of an OTS-treated oxidized silicon wafer, respectively.

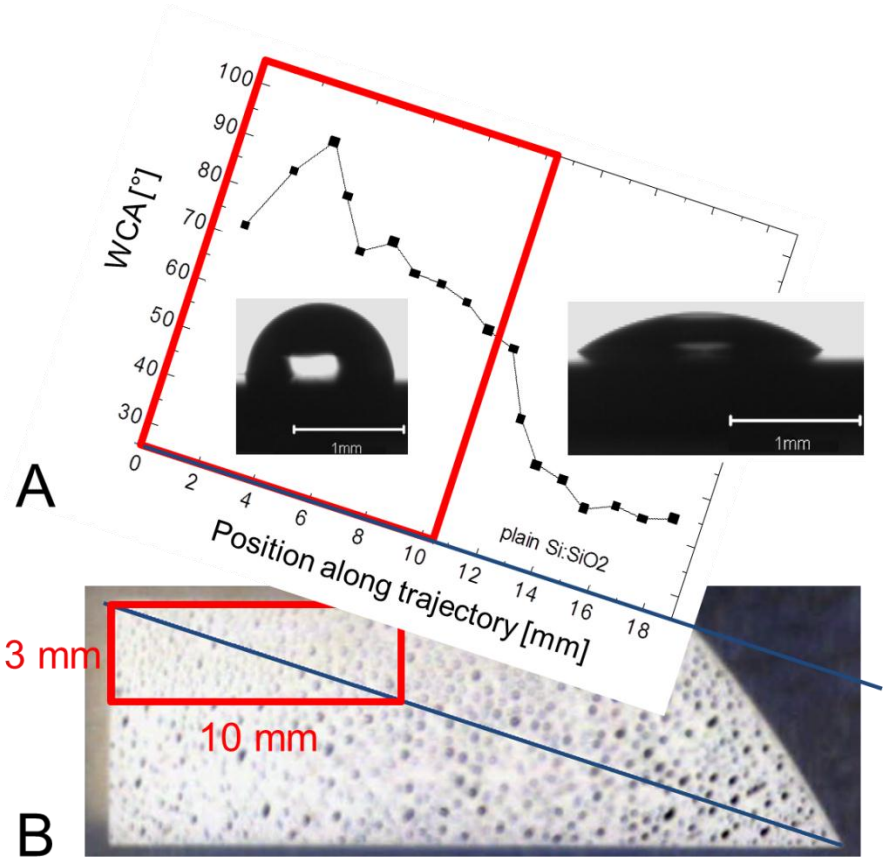

Figure A.5: A. Measured water contact angle along the diagonal of the printing area of inkjet-printed SAMs (from toluene, 0.5 mM OTS) on silicon oxide. B. Photographic image (top-view) of the oxidized silicon wafer.

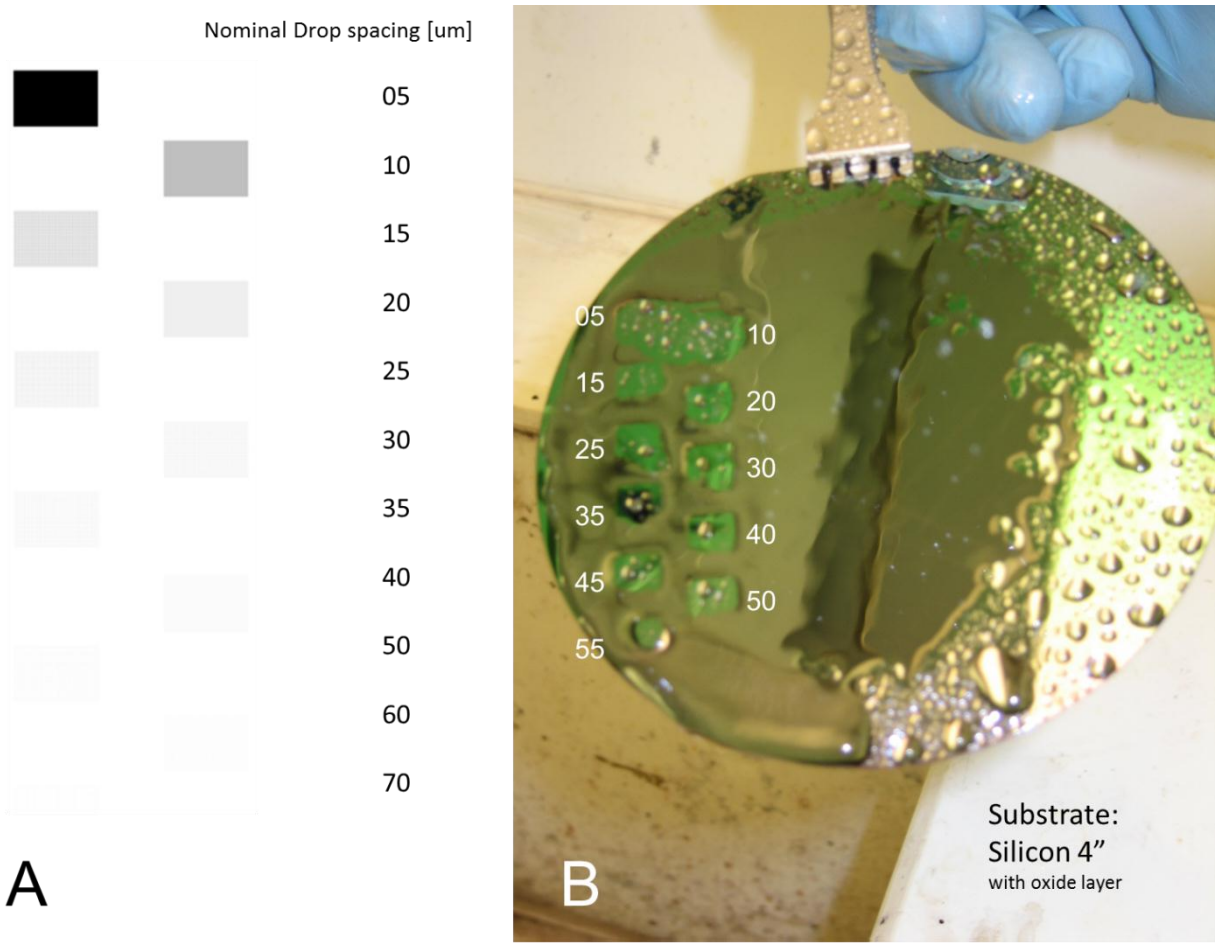

Figure A.6: A. Printing pattern with varying drop spacing. B. Photographic image of an oxidized silicon wafer with OTS molecular layers grown by inkjet printing of the pattern shown in A. The numbers indicate the drop spacing of the printing sub-pattern next to them. For this snapshot, deionized water was sprayed onto the wafer (photography courtesy of Zia Ullah Khan, Linköping University, Organic Electronics).

Chapter A.5: Evaporation of larger mesitylene droplets on a silicon oxide surface

For illustration, the evaporation of a 0.3 µL sessile mesitylene droplet from a reference silicon oxide surface was followed under normal conditions (temperature 25°C, RH 39 %) using a goniometer *OCA-20* (DataPhysics) equipped with video microscopy (Video A.1, **available as a separate file**). The video stream was analyzed afterwards with MATLAB to determine the base diameter and the height of the droplet in spherical-cap approximation as well as the contact angle from the tangents of the perimeter of the sessile droplet with the base line. Figure A.7 illustrates the image analysis process for one video frame. The volume of the droplet in any frame can be approximated from the determined geometrical parameters as shown in Figure A.8. More details (greyscale analysis, threshold values, reliability etc.) are found in the diploma thesis (Christian Belgardt: "Fabrication of microstructured OTS monolayers on silicon oxide surfaces", TU Chemnitz, 2012) accessible via URL **http://nbn-resolving.de/urn:nbn:de:bsz:ch1-qucosa-86379** (in German). Figure A.9 shows three frames of the video stream.

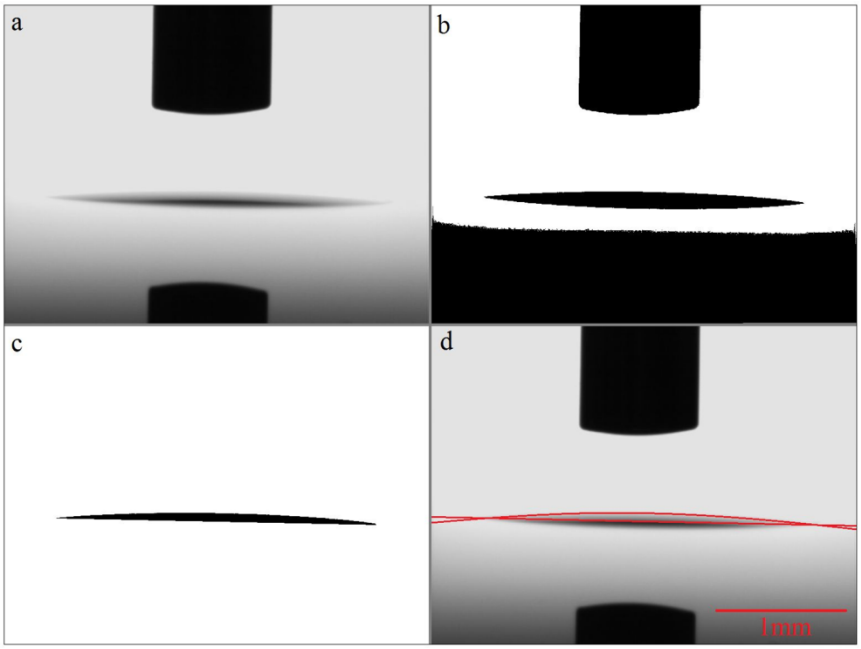

Figure A.7: Illustration of the image analysis algorithm applied to one frame out of a video stream: a) original frame; b) binarized frame; c) cropped projection of the droplet; d) fitted functions for substrate surface (base line) and perimeter of the droplet in spherical-cap approximation.

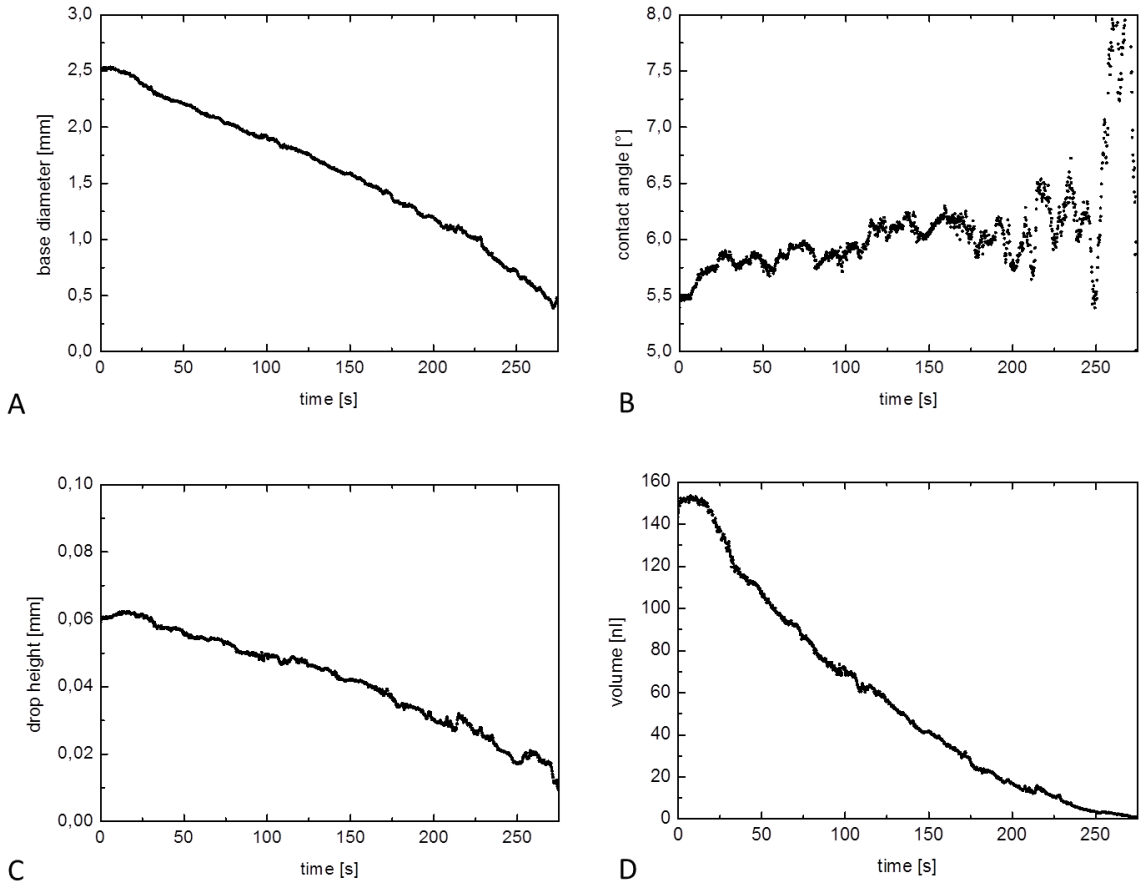

Figure A.8: Base diameter (A), contact angle (B) and droplet height (C) of an evaporating 0.3 µL mesitylene droplet on a silicon oxide surface, determined via video microscopy of a side view of the droplet and image analysis. The volume (D) is calculated from base diameter and droplet height in spherical cap geometry.

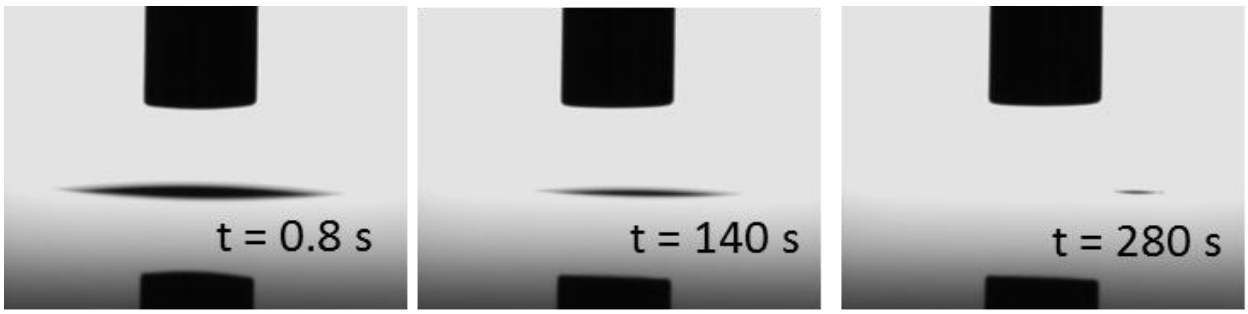

Figure A.9: Video frames at three different times 0.8 s, 140 s and 280 s showing the evaporation of the mesitylene droplet on silicon oxide with retreating contact line.

Chapter A.6: Thermodynamics of the evaporation of small sessile droplets

The change in the thermodynamics of a sessile droplet which has extensions in the µm range can be approximated by the Kelvin equation which describes the vapor pressure over a curved surface. It reads

$$RT \cdot \ln\left(\frac{p_k}{p_v}\right) = \frac{2 \cdot \gamma \cdot V_m}{r} \qquad \text{(A.3)}$$

where p_k is the vapor pressure over the flat surface (Kelvin pressure), p_v is the vapor pressure over the curved surface, γ is the surface tension (liquid/gas), V_m the molar volume of the liquid, r the radius of curvature (i.e. virtual radius of the sphere comprising the spherical cap), R the specific gas constant and T the temperature. Calculating p_v / p_k for the evaporating sessile droplet of our experiment (inkjet-deposited droplet of 10 pL after having changed shape from a sphere to a spherical cap) we find that the increase of the vapor pressure due to the curvature is lower than 0.005 % for the droplet in question (see Table A.2). The situation that certain parts of the evaporating droplet can be assigned a reduced temperature (in the range of 20 K) on account of the evaporation effects may explain changes of roughly the same quantity. From this viewpoint, the changed thermodynamics with decreasing droplet size should not play a role.

Table A.2: Increased vapor pressure due to increase of curvature for an evaporating inkjet-deposited droplet of 10 pL calculated after the Kelvin equation (Eq. A.3)

Drop volume	p_v / p_k
10.0 pL	1.00000660
5.0 pL	1.00000831
2.0 pL	1.00001126
1.0 pL	1.00001422
0.50 pL	1.00001790
0.20 pL	1.00002425
0.10 pL	1.00003026
0.05 pL	1.00003817
0.03 pL (@ 443 ns)	1.00004548